Ultramicroscopy 267 (2024) 114048

Contents lists available at ScienceDirect

Ultramicroscopy

journal homepage: www.elsevier.com/locate/ultramic

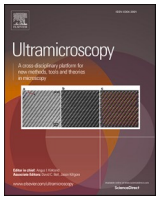

A new method for estimating nanoparticle deposition coverage from a set of weak-contrast SEM images

Bchara Sidnawi [a,b], Liang Zhao [a,c], Bo Li [a,c], Qianhong Wu [a,b,*]

[a] Department of Mechanical Engineering, Villanova University, PA 19085, USA
[b] Cellular Biomechanics and Sport Science Laboratory, Villanova University, PA 19085, USA
[c] Hybrid Nano-Architectures and Advanced Manufacturing Laboratory

ARTICLE INFO

Keywords:
SEM Imaging
Weak contrast
Image processing
Nanoparticle coverage

ABSTRACT

Imaging nanomaterials in hybrid systems is critical to understanding the structure and functionality of these systems. However, current technologies such as scanning electron microscopy (SEM) may obtain high resolution/contrast images at the cost of damaging or contaminating the sample. For example, to prevent the charging of organic substrate/matrix, a very thin layer of metal is coated on the surface, which will permanently contaminate the sample and eliminate the possibility of reusing it for following processes. Conversely, examining the sample without any modifications, in pursuit of high-fidelity digital images of its unperturbed state, can come at the cost of low-quality images that are challenging to process. Here, a solution is proposed for the case where no brightness threshold is available to reliably judge whether a region is covered with nanomaterials. The method examines local brightness variability to detect nanomaterial deposits. Very good agreement with manually obtained values of the coverage is observed, and a strong case is made for the method's automatability. Although the developed methodology is showcased in the context of SEM images of Polydimethylsiloxane (PDMS) substrates on which silicone dioxide (SiO_2) nanoparticles are assembled, the underlying concepts may be extended to situations where straightforward brightness thresholding is not viable.

1. Introduction

Nanomaterial-organic hybrid material systems have found extensive applications in composite, flexible and wearable electronics, energy storage systems, as well as medicine [1–5], etc. Many observational studies involve analyzing images for substrate coverage detection. Those may be underwater photographs to estimate the relative abundance of coral for example [6], lab images of biofilm coatings [7], or microscope digital images of substrates on which nanomaterials are deposited [8,9].

While imaging nanomaterials in hybrid systems is critical to understand the structure and functionality of these systems, it can be extremely challenging. Taking scanning electron microscopy (SEM) as an example, if the nanomaterials are deposited on top of or embedded into an organic substrate/matrix such as polymer or tissue, the charging of an organic (or even an inorganic) substrate can significantly disturb the imaging process. A common practice is to coat the surface with a thin conductive coating layer (e.g. metal) to eliminate charging and for biological samples, an additional dehydration process might be needed [10–12]. However, such processes could permanently contaminate or damage the sample and prevent it from further processing. Note that it is sometimes possible to remove the coating from SEM samples. Nevertheless, the coating removal process usually involves new chemicals. In the case of nanoparticle assembly where the same substrate needs to be imaged at different assembly times, the introduced chemicals for the coating removal may alter the surface properties of the substrate and/or nanoparticles and change the assembly kinetics. Furthermore, while nm resolution in FE-SEM with ionic liquid [13,14] can be achieved and some systems do not need conductive layer coating, such cases do not cover conditions where imaging technology reaches its limits for some hard-to-image samples. To image the pristine sample without conductive coatings, one can reduce the accelerating voltage or vacuum level at the cost of a compromised image resolution/contrast. When processing these digital images, such compromise creates difficulty for declaring whether a region is covered by the nanomaterials of interest, as a criterion for such an assessment would not be immediately obvious from the raw brightness data of the image and such conditions cannot be appropriately handled by existing software.

In a hybrid system, the coverage/content of nanomaterials on the

* Corresponding author at: 800 Lancaster Ave. Department of Mechanical Engineering, Villanova University, PA 19085, USA
E-mail address: qianhong.wu@villanova.edu (Q. Wu).

https://doi.org/10.1016/j.ultramic.2024.114048
Received 21 February 2023; Received in revised form 21 February 2024; Accepted 11 September 2024
Available online 14 September 2024

surface/cross section can be of great interests to establish the structure-property relationship. Therefore, many image processing efforts focus on coverage analysis. Image processing methods have also been reported for other applications. These include mixing time estimation from images of a stirred transparent tank [15], studying image contrast by analyzing Sum Frequency Generation Imaging Microscopy (SFGIM) images of monodentate and bidentate alkanethiol Self-Assembled Monolayers (SAMs) 16], background estimation for precisely localizing nanoscale light emitters [17], fast nanoparticle sizing using dynamic light scattering [18,19] and counting of needle-shaped crystals by applying t he Radon transform to their digital microscope images [20]. For seabed photographs [6], the random point count is a popular method for estimating a certain species coverage. A set of random points is overlaid on the photograph and a user visually flags the points that happen to be over the species of interest. From the number of those designated points, a statistical estimate of that species coverage is then made.

When it comes to processing microscope images for a substrate's covered fraction, the task consists of simply distinguishing empty regions from covered ones. More often than not, as in the case of the study by Carman and Budini cited earlier [8] for instance, the brightness contrast between empty and covered regions is high enough to easily determine a brightness threshold, below or above which a pixel can be designated as corresponding to a covered or a vacant area. However, such a clear cut through the brightness range is not always present. Sometimes, the overlap between the brightness ranges corresponding to empty and covered regions can be significant enough to throw off any coverage estimates based on simple brightness thresholding. Addressing such issues is typically attempted by contrast enhancement. A recently proposed model for image enhancement [21] has been shown to significantly improve the quality of raw underwater images in which high blurriness and color casts are often encountered. In the case discussed herein, however, as will be illustrated shortly, contrast enhancement can do little to make the regions of interest more distinguishable, at best, and can even exacerbate the problem, at worst.

As there are usually only two region categories to be distinguished on a substrate (either covered or empty), the random point count with visual detection can indeed serve the purpose, with more random pixels yielding a coverage estimate that is closer to the true value. However, when high accuracy is required for a substantial number of images, manual pixel selections for each of those images become onerous, and prohibitively time expensive. The importance of a special type of nanomaterials, 2D materials, has been elucidated in two recent reviews on their key role in strain engineering [22] and Surface-Enhanced Raman Spectroscopy (SERS) [23]. Novel, ecofriendly techniques of assembling 2D materials on flexible polymer substrates, for future hybrid flexible electronics applications, have also been recently reported [24,25]. Therefore, the prospect of flexible devices that involve nanomaterials, e.g., 2D materials assembled on flexible substrates[24,25], will necessitate future elaborate studies exploring ways to enhance the assembly speed and quality. This will inevitably entail a high volume of images to be assessed for coverage, highlighting the need for robust and automatable processing techniques. In this paper, a solution to the case when simple brightness thresholding is not enough, is proposed.

1.1. *Covered Fraction Detection*

Fig. 1a, shows an example that is representative of the kind of images that this communication is concerned with. In this SEM image, the grayscale brightness contrast between the covered and empty regions is not high enough to prevent the brightness ranges corresponding to those regions from significantly overlapping, or in this instance, one engulfing the other (Fig. 1b). Note the inside region of each particle which happens to be dimmer than the periphery and hence could be mistaken for an empty region. This renders simple brightness thresholding for coverage detection unreliable.

The top row of Fig. 2 shows a version of the image in Fig. 1a, where the covered regions were manually marked (Fig. 2a) in black (0 brightness value), next to another where the maxima have been located using the ImageJ software (Fig. 2b). Since no pixels in the empty regions are completely dark (see the red curve in Fig. 1), a quick count of the black pixels in the manually marked version yielded a coverage value of

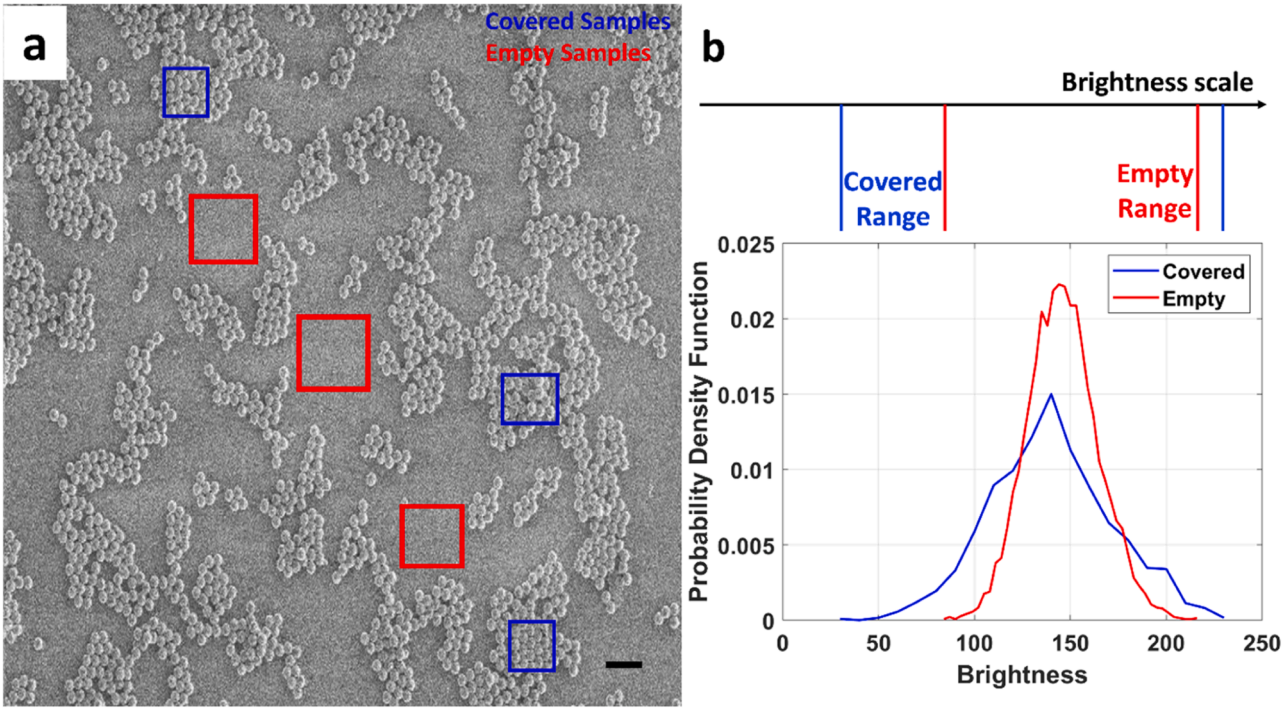

Fig. 1. (a): SEM image of a location on a substrate covered by silicon dioxide particles (glass beads). The red and blue squares enclose the manually sampled regions from the empty, and covered parts of the substrate, respectively. scale bar: 3 μm (b): The brightness distributions exhibited by the empty and covered regions.

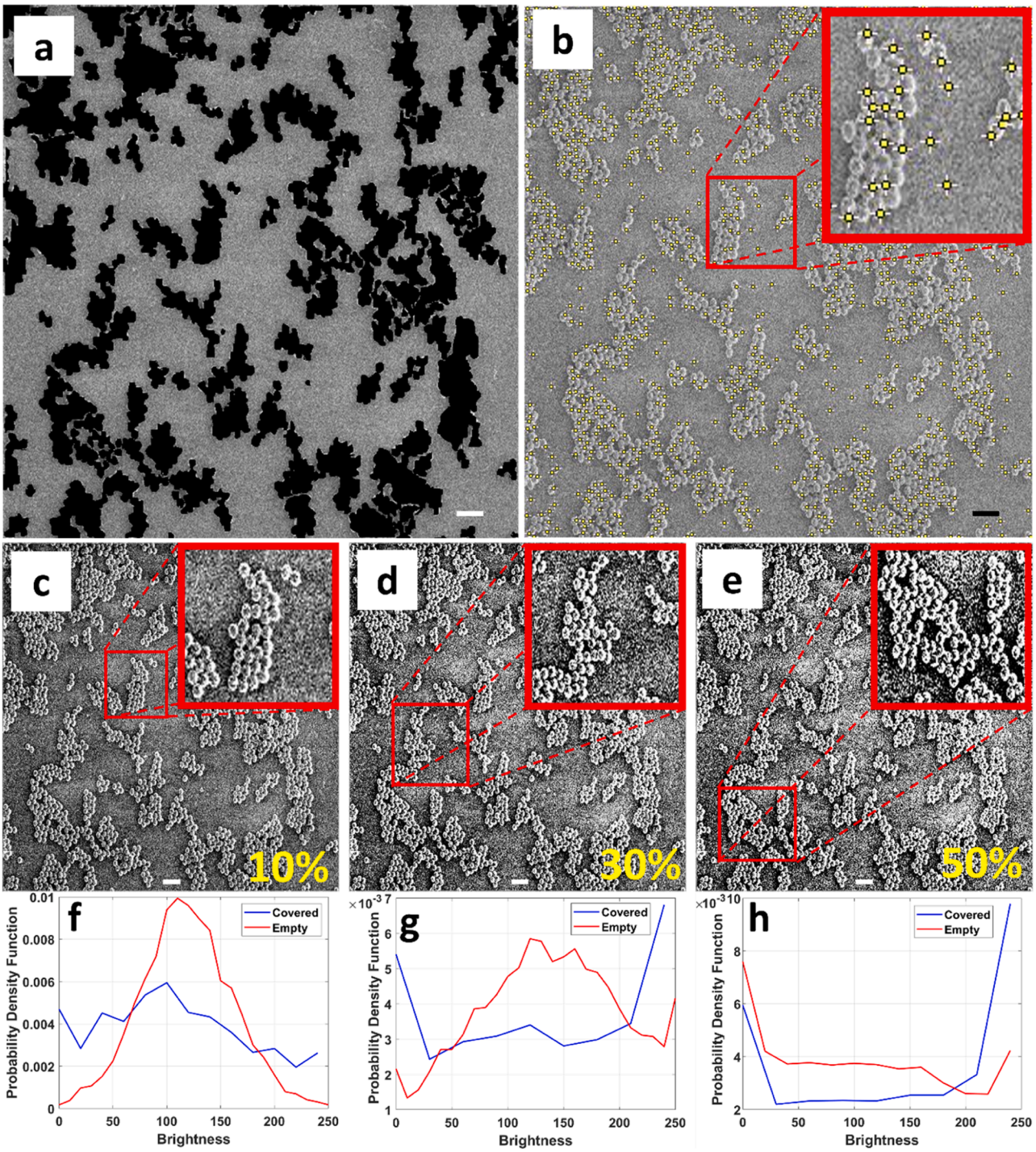

Fig. 2. (a): A manually marked version of the original image in Fig. 1a. (b): another version where maxima are located to seek particles. (c-e) Contrast-enhanced versions of the original image, at 10% (c), 30% (d), and 50% (e) saturated pixels. (f-h): The brightness distributions corresponding to the enhanced versions in (c-e). All scale bars: 3 μm.

0.2619. The maxima found using ImageJ still missed many particles while mistakenly marking locations in empty regions. The middle row (Fig. 2c-e) shows processed versions of the original image, where contrast has been enhanced in ImageJ. Although particle covered regions are much more pronounced, it can be seen how the problem is made worse. The particle peripheral regions are now much brighter than their interior, in addition to empty regions racking up more bright and dark pixels, thereby further widening the brightness range overlap, as confirmed by their corresponding distributions shown in the bottom row (Fig. 2f-h).

The data of the original image in Fig. 1 needs to be manipulated in a way such that a signal corresponding to the deposits stands out. If b_{ij} denotes the grayscale brightness value corresponding to the pixel in the i^{th} row and j^{th} column, $\bar{b}_{ij}$ is defined as the average value of b over a window that is centered around that pixel. The window's height and width are denoted as $2r_1 + 1$ and $2r_2 + 1$, respectively. $\bar{b}_{ij}$ is then given by Eq. 1.

$$\bar{b}_{ij} = \frac{\sum_{k=i-r_1}^{k=i+r_1}\sum_{l=j-r_2}^{l=j+r_2} b_{kl}}{(2r_1+1)(2r_2+1)} \tag{1}$$

The corresponding standard deviation would then be obtained as:

$$s_{ij} = \sqrt{\frac{\sum_{k=i-r_1}^{k=i+r_1}\sum_{l=j-r_2}^{l=j+r_2}\left(b_{kl}-\bar{b}_{ij}\right)^2}{(2r_1+1)(2r_2+1)}} \tag{2}$$

s_{ij} is normalized by its maximum value as $s^*_{ij} = \frac{s_{ij}}{\max(s_{ij})}$

Fig. 3b shows a color map of s^*_{ij} next to the original image (Fig. 3a). Note how in the color map, individual particles can be easily made out against the substrate. The values of r_1 and r_2 that made the particles so discernible in this example are $r_1 = 3$ and $r_2 = 3$. These values may vary depending on the image resolution and magnification. It is now clear that s^*_{ij} is the signal sought after for coverage detection. This becomes especially apparent when a map of s^*_{ij} is viewed in 3D as shown in Fig. 3c. Covered regions seem to feature sharp cliffs surrounded by empty regions. Let n be the total number of mapped pixels. The fraction $F(\tau)$ of pixels whose s^* value is above a certain threshold τ $(0 \le \tau \le 1)$ is then obtained as:

$$F(\tau) = \frac{\sum H\left(s^*_{ij} - \tau\right)}{n} \tag{3}$$

The summation in Eq. 3 is performed over all the mapped pixels, and H is the Heaviside step function. When τ gradually decreases from 1 to 0, F increases slowly until τ approaches 0, close to which the cliffs' bases would make F shoot up towards 1. Therefore, the coverage, which will be denoted as δ, would be the value of F around which its slope briefly stabilizes (due to the flat faces of the cliffs near their bases) before the sharp increase begins. In Fig. 3d, the x-axis is the threshold index representing τ as it decreases from 1 to 0 (in decrements of $1/1000$, which happens to provide enough resolution to compute the gradient in this instance). Compared to the value of 0.2619 computed earlier from the manually marked regions, the detected value in Fig. 3d is 0.2684, a hint to the technique's validity.

Fig. 4 shows the same procedure outlined above, but this time using the normalized brightness gradient magnitude, g^*_{ij}, instead of the s^*_{ij}. While Fig. 4a does show that gradient contours yield a signal that, at least visually, makes the deposits stand out, Fig. 4b reveals how poorly it does so compared to the significantly more pronounced contrast with which s^*_{ij} differentiates the empty and covered regions (Fig. 3c). This is further confirmed in Fig. 4c, where the featureless rise of the red curve makes it challenging to pinpoint any possible value for the coverage. It may be argued that a watershed method, which relies on gradients to identify shapes and objects, could be used to flag the particles by picking circular ridges in the gradient map then counting them. However, even if this were to be applied to the more discerning s^* map, the uncertainties brought on by distorted outlines of closely packed particles would still need to be dealt with, rendering the endeavor more complicated than it has to be. This is not to mention cases where the features of interest exhibit random, rather than regular and consistent shapes.

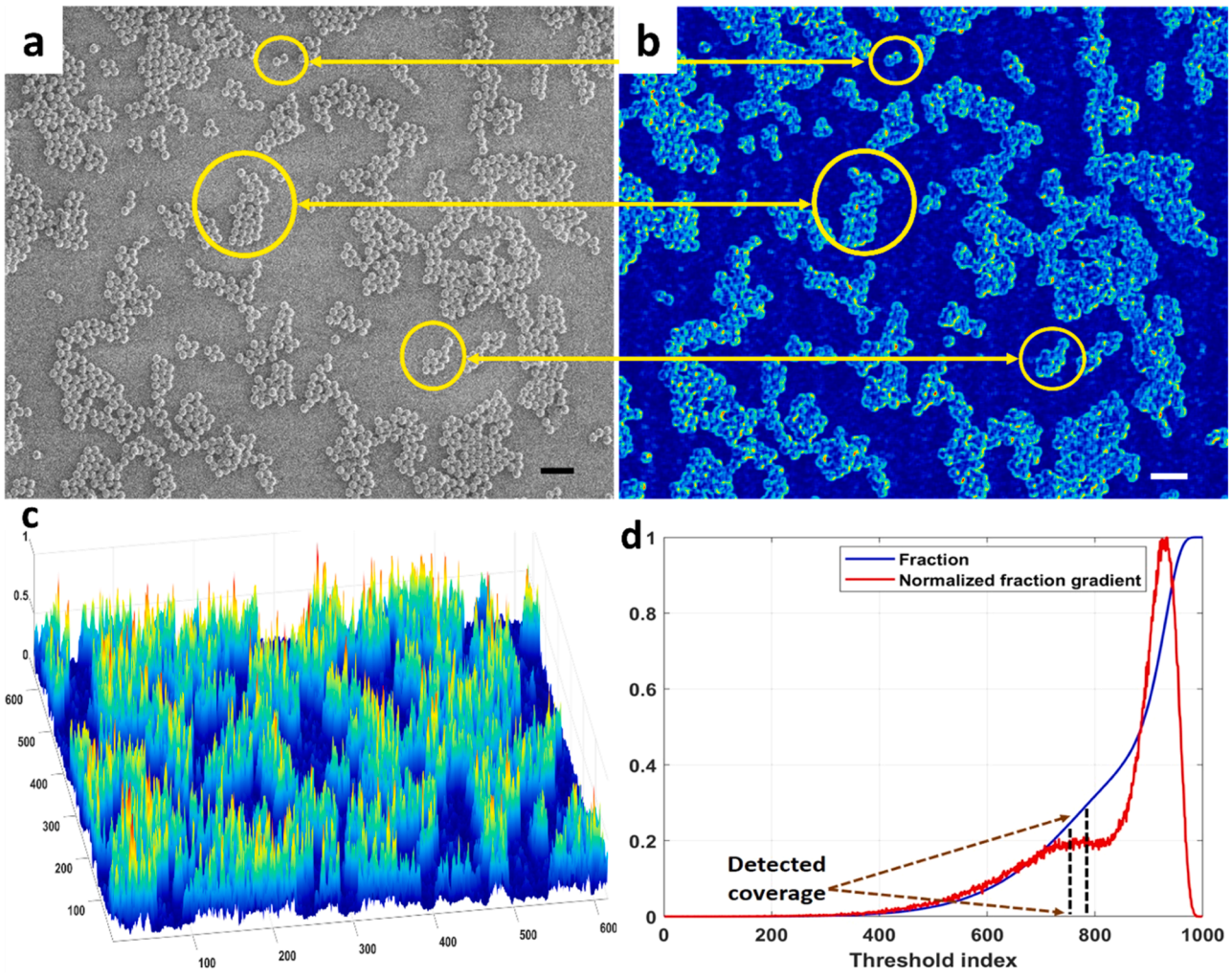

Fig. 3. (a) The original image next to its corresponding (b) color map of s^*_{ij} (a top view of c), (c) a surface plot of s^*_{ij}, (d) coverage detection. Scale bar: 3 μm.

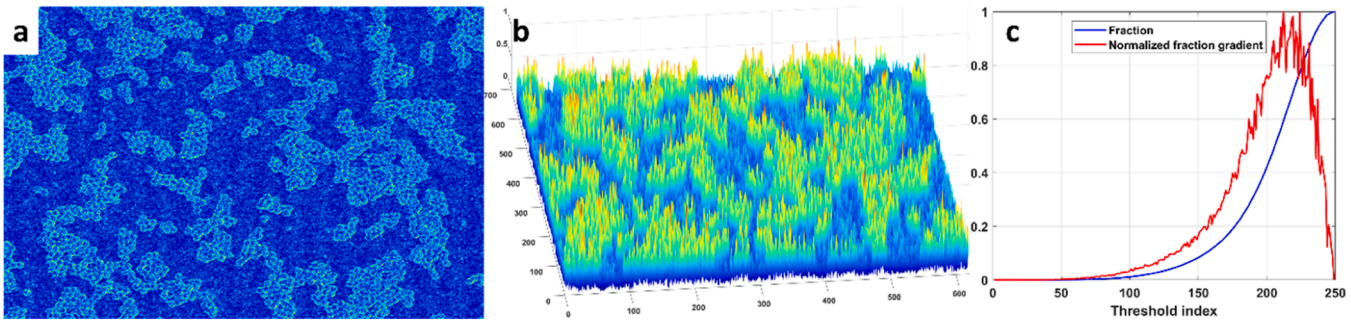

Fig. 4. (a) The normalized brightness gradient magnitude contours, (b) a 3D plot of the normalized gradient magnitude, and (c) $F(\tau)$ and its normalized gradient based on (b).

1.2. Automated detection

When hundreds, or even thousands of images such as the one shown in Fig. 1 need to be processed for coverage, manually performing the procedure developed in the previous section clearly becomes unrealistic. Therefore, some precisely quantifiable feature of $F(\tau)$ (Eq. 3) that can serve as a reliable predictor of δ, is worth pursuing. In the experimental work that entailed the use of such SEM imaging, 125 images were manually processed for δ, following the method described earlier. Preliminary mining of those results revealed an attribute of $F(\tau)$ that seems to predict δ reasonably well. Explicitly, it is the average value of F over an interval $a < \tau < b$ containing $\tau = 0.05$. This average value is denoted as $\overline{F}_{0.05}$.

$$\overline{F}_{0.05} = \frac{\int_a^b F(\tau)d\tau}{b-a} \tag{4}$$

Fig. 5 shows the correlation between $\overline{F}_{0.05}$ and δ as unraveled by the results from the 125 images, when the values of a and b were set to 0.04 and 0.09, respectively.

Barring the occasional scatter, the high R value of 0.99 reflects the tightness of this correlation.

The results shown in Fig. 3d, and Fig. 5 are not final. They illustrate a general method, as the values of r_1, r_2, a and b may still be optimized to make it as accurate as it can be. Optimization techniques are abundantly covered in the literature, and those parameters' optimal values pertaining to this specific set of 125 images, are not the focus of this study. Another set where the resolution, the particle (or feature) size, or the magnification are different would be expected to yield different optimal values. Whatever those values may be though, if they correspond to a subset of images that is representative enough of an entire set of interest, the resulting correlation can then be used to quickly estimate the coverage for the remainder of that set.

2. Conclusion

In conclusion, a method for substrate coverage detection in the case where simple brightness thresholding is not appropriate, is proposed and discussed. In the absence of a clear brightness contrast between covered and vacant regions, the high contrast of featureful deposits against a featureless substrate is quantified and used instead. The level of detail in the technical discussions should be enough for an interested reader to implement this method in any suitable coding language. Further expounding on the implementation side, this method clearly does not warrant a dedicated software package but can indeed be useful as a new tool to be added to any image processing software's toolbox.

CRediT authorship contribution statement

Bchara Sidnawi: Conceptualization, Formal analysis, Investigation, Methodology, Validation, Writing – original draft, Writing – review & editing. **Liang Zhao:** Data curation, Investigation, Writing – review & editing. **Bo Li:** Data curation, Investigation, Supervision, Writing – review & editing, Funding acquisition. **Qianhong Wu:** Conceptualization, Funding acquisition, Investigation, Methodology, Project administration, Resources, Supervision, Writing – review & editing.

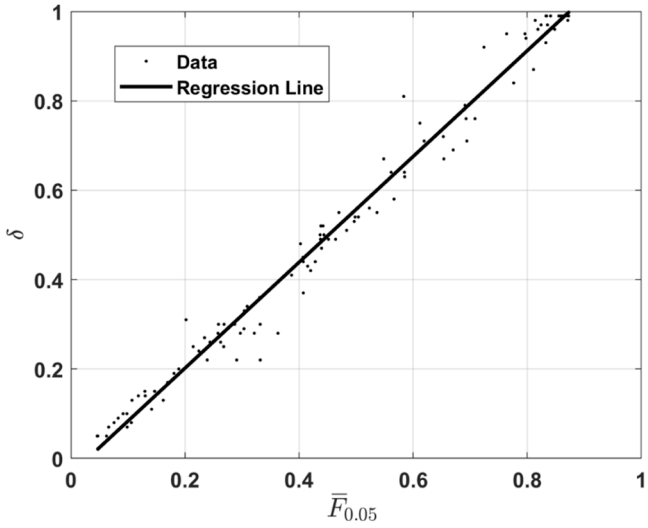

Fig. 5. The observed predictive correlation between δ and $\overline{F}_{0.05}$. Regression line: $\delta = 1.1837\overline{F}_{0.05} - 0.0348$, $R = 0.9914$.

Declaration of competing interest

The authors declare that they have no known competing financial interests or personal relationships that could have appeared to influence the work reported in this paper.

Data availability

The data that support the findings of this study are available from the corresponding author upon reasonable request.

Acknowledgement

This work is supported by the National Science Foundation's grant No. 2003077.

References

[1] M. Park, et al., Highly stretchable electric circuits from a composite material of silver nanoparticles and elastomeric fibres, Nat. Nanotechnol. 7 (2012) 803–809.

[2] C. Mandoli, et al., Stem cell aligned growth induced by CeO2 nanoparticles in PLGA scaffolds with improved bioactivity for regenerative medicine, Adv. Funct. Mater. 20 (2010) 1617–1624.
[3] He, J., Sill, K. & Xiang, H. Self-directed self-assembly of nanoparticle /copolymer mixtures. 55–59 (2005) doi:10.1038/nature03361.1.
[4] F. Brunetti, et al., Printed Solar Cells and Energy Storage Devices on Paper Substrates, Adv. Funct. Mater. 29 (2019).
[5] K.E. Mueggenburg, X.-M. Lin, R.H. Goldsmith, H.M. Jaeger, Elastic membranes of close-packed nanoparticle arrays, Nat. Mater. 6 (2007) 656–660.
[6] K.E. Kohler, S.M. Gill, Coral Point Count with Excel extensions (CPCe): A Visual Basic program for the determination of coral and substrate coverage using random point count methodology, Comput. Geosci. 32 (2006) 1259–1269.
[7] E. Ribeiro, et al., Automated image-based method for laboratory screening of coating libraries for adhesion of algae and bacterial biofilms, J. Comb. Chem. 10 (2008) 586–594.
[8] J. Caram, N. Budini, R.D. Arce, Analysis of substrate coverage of hybrid halide perovskite thin films deposited on glass, Rev. Mater. 23 (2018).
[9] R. Cao, T.T. Wang, G. DeMaria, J.K. Sheehan, M. Kesimer, Mapping the Protein Domain Structures of the Respiratory Mucins: A Mucin Proteome Coverage Study, J. Proteome Res. 11 (2012) 4013–4023.
[10] M.J. Russo, et al., Antifouling Strategies for Electrochemical Biosensing: Mechanisms and Performance toward Point of Care Based Diagnostic Applications, ACS Sensors 6 (2021) 1482–1507.
[11] J. Gibbons, P. Geetha-Loganathan, Processing embryo, eggshell, and fungal culture for scanning electron microscopy, J. Vis. Exp. (2019) 1–10. **2019**.
[12] Ul-Hamid, A. Sample Preparation BT - A Beginners' Guide to Scanning Electron Microscopy. in (ed. Ul-Hamid, A.) 309–359 (Springer International Publishing, 2018). doi:10.1007/978-3-319-98482-7_8.
[13] S. Kuwabata, A. Kongkanand, D. Oyamatsu, T. Torimoto, Observation of ionic liquid by scanning electron microscope, Chem. Lett. 35 (2006) 600–601.
[14] K. Horigome, T. Ueki, D. Suzuki, Direct visualization of swollen microgels by scanning electron microscopy using ionic liquids, Polym. J. 48 (2016) 273–279.
[15] F. Cabaret, S. Bonnot, L. Fradette, P.A. Tanguy, Mixing time analysis using colorimetric methods and image processing, Ind. Eng. Chem. Res. 46 (2007) 5032–5042.
[16] J.H. Jang, J. Jacob, G. Santos, T.R. Lee, S. Baldelli, Image contrast in sum frequency generation microscopy based on monolayer order and coverage, J. Phys. Chem. C 117 (2013) 15192–15202.
[17] C.Y. Cheng, C.L. Hsieh, Background Estimation and Correction for High-Precision Localization Microscopy, ACS Photonics 4 (2017) 1730–1739.
[18] C. Xu, X. Cai, J. Zhang, L. Liu, Fast nanoparticle sizing by image dynamic light scattering, Particuology 19 (2015) 82–85.
[19] D. Zhang, X. Cai, W. Zhou, Two-dimensional self-adapting fast Fourier transform algorithm for nanoparticle sizing by ultrafast image-based dynamic light scattering, Particuology 41 (2018) 74–84.
[20] J.X. Wu, et al., Image analytical approach for needle-shaped crystal counting and length estimation, Cryst. Growth Des. 15 (2015) 4876–4885.
[21] C. Li, et al., An Underwater Image Enhancement Benchmark Dataset and beyond, IEEE Trans. Image Process. 29 (2020) 4376–4389.
[22] Z. Dai, L. Liu, Z. Zhang, Strain Engineering of 2D Materials: Issues and Opportunities at the Interface, Adv. Mater. 31 (2019) 1–11.
[23] M. Chen, et al., 2D materials: Excellent substrates for surface-enhanced Raman scattering (SERS) in chemical sensing and biosensing, TrAC - Trends Anal. Chem. 130 (2020) 115983.
[24] D. Zhou, et al., Sono-Assisted Surface Energy Driven Assembly of 2D Materials on Flexible Polymer Substrates: A Green Assembly Method Using Water, ACS Appl. Mater. Interfaces 11 (2019) 33458–33464.
[25] D. Zhou, et al., Ultrafast assembly and healing of nanomaterial networks on polymer substrates for flexible hybrid electronics, Appl. Mater. Today 22 (2021).